Available online at www.sciencedirect.com

ScienceDirect

Journal of the Franklin Institute 352 (2015) 577–602

Journal of The Franklin Institute

www.elsevier.com/locate/jfranklin

A robust wheel slip ratio control design combining hydraulic and regenerative braking systems for in-wheel-motors-driven electric Vehicles

Bin Wang[a,b], Xiaoyu Huang[b], Junmin Wang[b,*], Xuexun Guo[a], Xiaoyuan Zhu[b]

[a]*Hubei Key Laboratory of Advanced Technology of Automotive Parts, Wuhan University of Technology, Wuhan 430070, China*

[b]*Department of Mechanical and Aerospace Engineering, Ohio State University, Columbus, OH 43210, USA*

Received 6 January 2014; received in revised form 6 June 2014; accepted 10 June 2014
Available online 20 June 2014

Abstract

This paper develops a robust wheel slip controller for in-wheel-motors-driven electric vehicles equipped with both hydraulic anti-lock braking systems (ABS) and regenerative braking (RB) systems. Based on a combination of optimal predictive control design and Lyapunov theory, the issue of uncertain vehicle parameters is well addressed. A novel braking torque distribution strategy is also introduced to achieve smooth regulation of the hydraulic pressure, such that pedal pulsating effect of the traditional ABS system can be relieved. By utilizing the larger working range of the hydraulic braking (HB) system and the faster response of the RB system, a better wheel slip control performance can be obtained. Moreover, the torque distributer helps to reach a good compromise between braking distance and the magnitude of the RB torque, which is directly related to the amount of regenerated energy. The effectiveness of the proposed control system has been validated in various simulations.

1. Introduction

Anti-lock braking system (ABS) plays a crucial role in vehicle emergency braking maneuvers because it helps to maintain the wheel slip near a desired value to avoid loss of directional

*Corresponding author.
E-mail address: wang.1381@osu.edu (J. Wang).

http://dx.doi.org/10.1016/j.jfranklin.2014.06.004
0016-0032/

Nomenclature

A_{vi}	cross-sectional area of the inlet valve
A_{vd}	cross-sectional area of the outlet valve
A_w	wheel cylinder cross sectional area
C_d	flow coefficient of the inlet of the valve
f_v	viscous friction coefficient
f_a	aerodynamic drag coefficient
f_{hb}	brake friction coefficient
F_a	aerodynamic drag force
F_ω	wheel viscous friction force
F_x	tire road friction force
g	gravitational acceleration
I_b	motor current
J	moment of inertia of tire/wheel/motor set
k	bulk modulus of the brake oil
m	total mass of the quarter vehicle
p_w	wheel cylinder pressure
p_m	master cylinder pressure
p_0	reservoir pressure
P_{motor}	power generated by regenerative braking system
Q_c	battery energy capacity
r_{hb}	effective brake radius
r_{eff}	tire effective radius
R_b	equivalent battery internal resistant
SOC_{act}	actual battery SOC value
SOC_{ini}	initial battery SOC value
T_{act}	actual braking torque
T_{hb}	friction brake torque
T_b	control input
t	time
U_{out}	battery output voltage
U_{op}	open-circuit voltage
v	vehicle velocity
V_0	volume under no pressure
ω_w	wheel angular speed
ω_v	scaled vehicle speed
μ	friction coefficient
λ	slip ratio
ρ	power efficiency
φ_i	coefficient of increase mode
φ_d	coefficient of decrease mode

control, and at the same time generate a tire-road friction force as large as possible to reduce the braking distance [1]. In a conventional hydraulic braking (HB) system, the hydraulic pressure

can be controlled by regulating the solenoid valves through pulse width modulated (PWM) signals to avoid locking the wheels. The HB torque can have a very large working range upon pressure variations. While due to the low carrier pulse frequency in a conventional ABS system, the frictional brake torque is slow in dynamics and always has a significant delay during a transient response, which seriously affects the slip control performance. For a regenerative braking (RB) system, it has a relatively limited working range that may be insufficient for the required brake torque; however, the electric motor in a RB system features a much faster bandwidth, which can benefit the wheel slip control in an emergency-braking maneuver. In addition, the energy wasted by the conventional friction brake can be partially restored by the RB system. Therefore, the blending slip control has attracted much attention from both industry and academia [2–10]. Some research about the hybrid HB and RB system are mainly focused on improving the energy recovery performance [4–6,9]. Research in [7] studied the hybrid ABS system on an electrified bus and proposed a performance index to compute the total brake torque and an optimization strategy for brake torque distribution. However, the proposed strategy failed to take full advantage of RB system so that no regenerative energy factor was considered. A permanent magnet synchronous motor (PMSM) model for RB system was built and the brake distribution strategy was achieved by an ideal brake-proportioning curve in [8]. However, the literature neglected the slip ratio–friction relationship, which was vital since under different slip ratios the tire-road friction can be varied significantly. Research in [11] used the sliding mode control (SMC) into the blending ABS system and through the utilization of continuously variable transmission (CVT) to figure out the wheel speed fluctuating problem. However, the literature details very little on how to split the torque between the conventional ABS and RB system. A fuzzy logic control strategy is proposed in [12] to control the RB torque. The strategy has been investigated on a road test. The modeling of mechatronic systems can be difficult in practice due to the unknown disturbances and system complexity, researches in [13–15], in contrast to the model-based approach, utilize the data-driven approach to obtain the system model. A model-data integrated framework is proposed in [16], which provides a new approach on modeling the braking system.

In this paper, we design a novel hybrid ABS system for in-wheel-motors-driven electric vehicles (IWMDEVs) [3,4,46]. Owing to the special structure of IWMDEVs, the braking system is no longer a stand-along system just to provide a sufficient braking torque, but a subsystem where each wheel can be controlled by a high-level controller individually. Therefore, both the vehicle braking performance and energy efficiency can be improved. When it comes to the torque distribution between the HB and RB systems, the system characteristics need to be considered closely. For the HB system, we design a constant desired HB torque such that the pedal pulsating effect of the traditional ABS system can be relieved, and also help to reduce the hydraulic braking torque tracking error. At the same time, the RB system can help to track the fast-changing desired torque precisely.

The main contribution of this paper lies in three aspects. First, a novel robust controller that has satisfactory wheel slip tracking capability is designed; meanwhile, the robustness towards uncertain vehicle parameters is guaranteed. Second, this is among the first attempts to propose a torque distribution strategy for HB-RB blending ABS systems. By utilizing the large working range of the HB system and the fast response of the RB system, the hybrid ABS system can generate the desired brake torque dictated by the upper-level supervisory controller rapidly and smoothly. Third, the typical driver's pedal pulsating feeling during ABS operations is also well addressed. Pedal pulsating affects the judgment and feeling of drivers, and it may cause danger during emergency braking maneuvers. By the control strategy proposed in this paper, this problem is treated without changing the structure of the conventional pedal.

The rest of the paper is organized as follows. In Section 2, the models for regenerative braking system, hydraulic braking system, quarter-vehicle dynamics, and tire model are described. In Section 3, we introduce an optimal predictive control law for slip control under the assumption that no variation exists in system parameters, then a robust controller concerning the variation of the system parameters is proposed based on Lyapunov theory. With the consideration of hydraulic dynamics and driving feeling, a new torque distribution strategy is designed in Section 4. Simulation results and analyses of the proposed control system are given in Section 5.

2. System modeling

Wheel slip control systems have been studied for many years. The performances of these systems vary widely owing to different structures of the actuators, tire-road contact conditions, and the control strategies. For EVs with in-wheel motors, each wheel can be controlled independently. The hydraulic friction braking system on each wheel can work alone or together with a secondary regenerative braking system [4]. The slip control problem can therefore be analyzed by a quarter-car model. In this section, we first briefly describe the RB system. Then, the model of the HB system is constructed; a quarter-vehicle dynamics model and a tire model will also be presented.

2.1. Regenerative braking system

The in-wheel motors equipped on the prototype EV are customized permanent-magnet brushless DC motors, as shown in Fig. 1. The power source of the IWMDEV is a 72V lithium-ion battery pack. By running the in-wheel motors at the RB mode, the battery pack can be charged. The efficiency map of the RB system has been generated by vehicle chassis dynamometer tests [3]. In real-world applications, the control of regenerative braking can be realized via commercialized motor controllers. In this paper we assume that the RB torque can be precisely generated within the maximal and minimal motor torque limitations. Detailed modeling and characteristics descriptions of the RB system can be found in reference [3].

The power into the motor can be calculated as Eq. (1)

$$P_{motor}(t) = T_{act}(t) \cdot \omega_w(t) \cdot \rho(T_{act}, \omega_w) \tag{1}$$

Fig. 1. In-wheel motor of the prototype EV.

where P_{motor} is the power generated by regenerative braking system; T_{act} is the actual braking torque; ω_w is the wheel speed and $\rho(T_{act}, \omega_w)$ denotes the power efficiency, which is a function of the motor torque and speed. The efficiency $\rho(T_{act}, \omega_w)$ can be obtained by dynamometer tests under different command voltages and wheel speeds [4].

Based on a resistive Thevenin equivalent circuit model [12], the battery state of charge (SOC) is modeled as

$$SOC_{act} = SOC_{ini} - \frac{100 \int_0^t I_b(\tau) d\tau}{Q_c} \tag{2}$$

$$I_b = \frac{U_o - \sqrt{P_{motor} R_b}}{R_b} \tag{3}$$

where SOC_{act} is the actual battery SOC value; SOC_{ini} is the initial battery SOC value; Q_c is the total battery energy capacity.$U_{out} = \sqrt{P_{motor} R_b}$, U_{op} are the battery output voltage and open-circuit voltage, respectively; R_b is the equivalent battery internal resistant; I_b is the motor current.

2.2. Hydraulic system model

Apart from the regenerative braking, the hydraulic braking system, which is the main source of the braking force, can also be available on the IWMDEV. The HB system consists of five major components: master cylinder, wheel cylinder, reservoir, and inlet and outlet valves, as illustrated in Fig. 2. The inlet values are normally open and the outlet valves are normally closed. Once the driver steps on the braking pedal, the pressure in the master cylinder increases immediately. The pressure in the wheel cylinder will then increase sharply via the inlet valve. When holding the pressure, both inlet and outlet valves will be closed. When the pressure in the wheel cylinder needs to be reduced (e.g. electronic control unit finds that wheel locking is happening), the normally closed outlet valves will be opened upon control signals, and brake oil is released to the reservoir. The brake oil will ultimately be withdrawn back to the master cylinder by an oil pump when the reservoir tends to be full. This HB system performs ABS-like function by alternating pressure increase, pressure holding, and pressure decrease. The pressure can be measured by a pressure sensor.

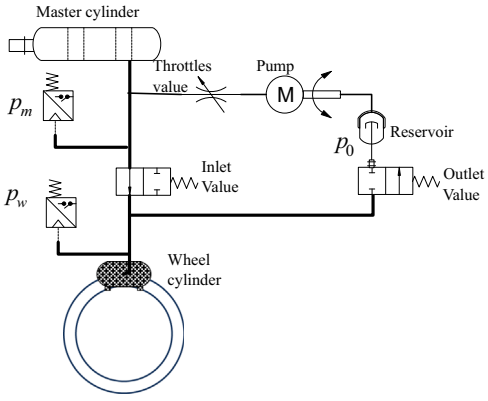

Fig. 2. Hydraulic braking system of the prototype EV.

In this paper, the hydraulic system is described by the following Eq. [12–19]:

$$\dot{p}_w(t) = \frac{\kappa_1 C_d A_{vi} k}{V_0}(p_m - p_w(t))^{\varphi_i} - \frac{\kappa_2 C_d A_{vd} k}{V_0}(p_w(t) - p_0)^{\varphi_d}. \tag{4}$$

where p_w, p_m, p_0 are wheel cylinder pressure, master cylinder pressure, and the reservoir pressure respectively and can be measured by pressure sensors as shown in Fig. 2. C_d, A_{vi}, A_{vd}, k and V_0 are the flow coefficient of the valves, the cross-sectional area of the inlet valves, the cross-sectional area of the outlet valves, the bulk modulus of the brake oil and the brake oil volume under no pressure respectively. φ_i and φ_d are the coefficients for pressure increase and decrease modes, respectively, and they can be calibrated from experimental data [12].

In order to simulate the on–off feature of the pressure modulation for the wheel cylinder, three modes of the HB system are introduced: increase, decrease, and holding, as shown in Table 1, where κ_1, κ_2 represent the control signals. The inlet and outlet solenoid valves are controlled by PWM signals [18].

With the wheel cylinder pressure obtained in (4), the HB torque can then be calculated using the following equation:

$$T_{hb}(t) = 2p_w(t)A_w f_{hb} r_{hb} \tag{5}$$

where $T_{hb}, A_w, f_{hb}, r_{hb}$ are the friction brake torque, wheel cylinder cross sectional area, the friction coefficient, and the effective brake radius, respectively.

2.3. Quarter vehicle dynamics model

In this section, we review a mathematical model for a quarter vehicles, which can be presented by a single wheel, as shown in Fig. 3, see also in [20,21]. Only a straight-line braking maneuver is considered, as in most of the existing ABS control strategies [22,23].

The dynamics of the quarter vehicle can be described as follows:

$$J\dot{\omega}_w(t) = -T_b(t) + r_{eff}(F_x(t) - F_\omega(t)), \tag{6}$$

$$m\dot{v}(t) = -F(t)_x - F_a(t), \tag{7}$$

$$F_a(t) = f_a v(t)^2, \tag{8}$$

$$F_\omega(t) = f_v \omega_w(t), \tag{9}$$

$$F_x(t) = \mu(\lambda) mg, \tag{10}$$

where T_b is the braking torque, F_x is the road friction brake force, v is vehicle velocity, r_{eff} is tire effective radius,J is the moment of inertia of tire/wheel/motor set, $g$is the gravitational acceleration, m is total mass of the quarter vehicle, F_ω is the wheel viscous friction force, and f_v

Table 1
Three modes of hydraulic braking system.

Mode	κ_1	κ_2
Pressure increasing	1	0
Pressure decreasing	0	1
Pressure holding	0	0

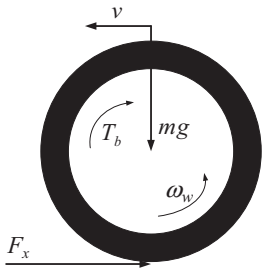

Fig. 3. Wheel dynamic model.

Table 2
Parameters of the tire model for various surfaces.

Surface condition	c_1	c_2	c_3
Wet asphalt	0.857	33.822	0.347
Dry concrete	1.1973	25.168	0.5373
Cobble dry	1.3713	6.4565	0.6691
Snow	0.1946	94.129	0.0646

is the wheel viscous friction coefficient,F_a is the aerodynamic drag force and f_a is the aerodynamic drag coefficient, μ is the tire-road friction coefficient, in connection with the slip ratio λ. A large number of empirical or analytical tire models have been developed in the literature [24,25]. In this paper, a widely used longitudinal $\mu-\lambda$ relationship is adopted, as expressed in (11).

$$\mu(\lambda) = c_1(1-e^{-c_2\lambda}) - c_3\lambda \tag{11}$$

where parameters of this tire model c_1, c_2, c_3 for different road surfaces are listed in Table 2 [25].

Substituting (8)–(10) into (6) and (7) gives

$$\dot{\omega}_v(t) = -\mu(\lambda)\frac{g}{r_{eff}} - \frac{f_a r_{eff}}{m}\omega_v(t)^2 \tag{12}$$

$$\dot{\omega}_w(t) = \frac{r_{eff}}{J}\mu(\lambda)mg - \frac{r_{eff}f_v}{J}\omega_w(t) - \frac{T_b(t)}{J} \tag{13}$$

where $\omega_v(t) = v(t)/r_{eff}$ is a scaled vehicle speed, which can be measured by dual-antenna global positioning system [26] or estimated by observers like the one in [27]. Since numerous studies have been devoted to the estimation of tire-road friction coefficient (TRFC) [24], the detailed methods will be omitted here. The longitudinal slip ratio λ during a braking maneuver is defined by

$$\lambda(t) = \frac{(\omega_v(t)-\omega_w(t))r_{eff}}{\omega_v(t)r_{eff}} = 1 - \frac{\omega_w(t)}{\omega_v(t)}. \tag{14}$$

Then, substituting (6)–(13) into the first derivative of (14) yields:

$$\dot{\lambda}(t) = \frac{1}{\omega_v(t)}((1-\lambda(t))\dot{\omega}_v(t) - \dot{\omega}_w(t))$$

$$= \frac{1}{\omega_v(t)}\left\{ \left[-\frac{g}{r_{eff}}(1-\lambda(t)) - \frac{r_{eff}}{J}mg \right]\mu(\lambda) + \frac{r_{eff}f_v}{J}\omega_w(t) - (1-\lambda(t))\frac{f_a r_{eff}}{m}\omega_v^2(t) \right\} + \frac{T_b(t)}{\omega_v(t)J} \tag{15}$$

This is a nonlinear model that represents bulk of the wheel-vehicle dynamics during a braking maneuver. The delay in the hydraulic actuator dynamics will be discussed in Section 5. The wheel slip control system will be designed in the following section.

3. Design of robust controller

The main control objective in this study is to regulate the wheel longitudinal slip ratio, in the presence of system parametric uncertainties. A robust controller is therefore proposed in this section to deal with the modeling errors caused by insufficient knowledge of the vehicle parameters. It is assumed that the set-point for the wheel slip has been generated by some high-level controller and is known in advance, as reported in [28].

Dynamic models (12) and (13) can be written as

$$\dot{x}_1 = f(x_1) + \mu(\lambda)\varepsilon_1, \tag{16}$$

$$\dot{x}_2 = f(x_2) + \mu(\lambda)\varepsilon_2 - T_b\varepsilon_3, \tag{17}$$

where $x_1 = \omega_v(t), x_2 = \omega_w(t)$, and

$$f(x_1) = -f_a r_{eff} {x_1}^2/m, \tag{18}$$

$$f(x_2) = -r_{eff}f_v x_2/J, \tag{19}$$

$$\varepsilon_1 = -g/r_{eff}, \tag{20}$$

$$\varepsilon_2 = r_{eff}\ \mathrm{mg}/J, \tag{21}$$

$$\varepsilon_3 = 1/J. \tag{22}$$

By substituting Eqs. (18)–(22) into (15), we have:

$$f(X) = \{(1-\lambda)f(x_1) + [\varepsilon_1(1-\lambda) - \varepsilon_2]\mu(\lambda) - f(x_2)\}/x_1. \tag{23}$$

Then, based on (23), (16) can be written as

$$\dot{\lambda} = f(X) + bu(t), \tag{24}$$

$$y = \lambda, \tag{25}$$

where

$$f(X) = \{(1-\lambda)f(x_1) + [\varepsilon_1(1-\lambda) - \varepsilon_2]\mu(\lambda) - f(x_2)\}/x_1, \tag{26}$$

$$X = [x_1 \ \ x_2]^T,$$

$$b = \varepsilon_3/x_1, \tag{27}$$

$$u(t) = T_b(t). \tag{28}$$

Remark 1. In this paper the slip ratio controller works only when the vehicle speed $x_1 > 0$, as in [1,11,18]. Actually, the anti-lock braking system will be deactivated at very low speeds [29,30].

3.1. Optimal predictive control law

When vehicle parameters are exactly known and vehicle states are accurately measured, an optimal predictive control (OPC) law can be applied for this specific problem [31,32]. The main idea is explained as follows.

The wheel slip of the next time instant $\overline{\lambda}(t+h)$ is first approximated by truncating the Taylor expansion up to the first order term, that is:

$$\overline{\lambda}(t+h) = \lambda(t) + h[\dot{e} + \dot{\lambda}(t)], \tag{29}$$

where h denotes the predictive period and is a real positive number [31]; $e = \lambda(t) - \lambda_d(t)$ and $\overline{\lambda}_d(t+h)$ can also be expressed in a similar way. Since the main objective is to reduce the slip tracking error with the minimum control effort if possible, a cost function is designed as follows:

$$\begin{aligned} \Theta &= \tfrac{1}{2}\tau_1[\overline{\lambda}_3(t+h) - \overline{\lambda}_d(t+h)]^2 + \tfrac{1}{2}\tau_2 u^2 \\ &= \tfrac{1}{2}\tau_1[e + h(f(X) - \dot{\lambda}_d) + hbu]^2 + \tfrac{1}{2}\tau_2 u^2, \end{aligned} \tag{30}$$

where $\tau_1 > 0$, $\tau_2 > 0$ are weighting factors that are associated with the relative importance of the penalized terms, namely, wheel slip tracking error and the brake torque. Based on (30), the necessary condition for the optimality is $\partial\Theta/\partial u = 0$, which leads to:

$$u(t) = -\frac{h\hat{b}}{h^2\hat{b}^2 + \eta}\left[e + h(\hat{f}(X) - \dot{\lambda}_d)\right], \tag{31}$$

where $\eta = \tau_2/\tau_1$. If vehicle parameters are exactly known, $\hat{f}(X)$ is equal to the nominal value $f(X)$ and $\hat{b}$ is equal to the nominal value b. Nevertheless, in real-world applications, numerous factors may affect the acquisition of actual vehicle parameters, for example, payload changes, under-inflated tires, and so on. It is however well known that robust controller is capable of dealing with modeling errors. Hence, in the following, we will first propose a robust control law based on (31), and then the stability of the overall system will be analyzed.

3.2. Robust control law

To deal with the uncertainties in $f(X)$, we propose a robust control law following the main ideas in [32–35]. Several important assumptions are first presented.

Assumption 1. The parameters subjected to uncertainties have known bounds, which yields:

$$|f(X)| \le \zeta\alpha^T\beta(t) \tag{32}$$

where

$$\alpha^T = [f_a r_{eff}/\mathrm{mg}/r_{eff}\ \ \mathrm{mg}\ r_{eff}/J\ \ r_{eff}f_v/J], \tag{33}$$

$$\beta^T = \left[\left|x_1(1-\lambda)\right| \quad \left|\frac{\mu(\lambda)(1-\lambda)}{x_1}\right| \quad \left|\frac{\mu(\lambda)}{x_1}\right| \quad \left|\frac{x_2}{x_1}\right|\right]. \tag{34}$$

Note that the vector $\alpha$is composed of vehicle parameters that are positive constants and $\zeta \geq \zeta_0 = \varepsilon_3/\hat{\varepsilon}_3$.

Assumption 2. $\dot{\lambda}$ is the derivative of the slip ratio and is assumed to be bounded, hence, there exists a positive constant P such that $|f(X)-\dot{\lambda}| \leq P$.

Assumption 3. Although accurate vehicle parameters may not be available, it is always possible to generate a comfortable "guessed" value for the vector α based on observations and common sense. The error between the guessed $\hat{f}(X)$ and the nominal value $f(X)$ is assumed to be bounded by a positive constant Ψ

$$|f(X)-\hat{f}(X)| \leq \Psi. \tag{35}$$

Now define $\xi = hb/(h^2\hat{b}^2+\eta)$ (where, $\eta = \tau_2/\tau_1 > 0$) and substitute (31) into (24), we have:

$$\dot{e} = -\frac{e}{h} + \left(\frac{1-\xi\hat{b}h}{\xi\hat{b}h}\right)(f(X)-\dot{\lambda}) + (f(X)-\hat{f}(X)). \tag{36}$$

Select a Lyapunov function candidate as

$$V(t) = \tfrac{1}{2}(\lambda(t)-\lambda_d(t))^2. \tag{37}$$

Its time derivative is calculated as

$$\dot{V}(t) = e\dot{e} = -\frac{e^2}{h} + e\left[\left(\frac{1}{\xi\hat{b}h}-1\right)(f(X)-\dot{\lambda}) + (f(X)-\hat{f}(X))\right].$$

Considering Assumption 2 and (35), when$e>0$,

$$\dot{V}(t) \leq -\frac{e^2}{h} + e\left[\left(\frac{1}{\xi\hat{b}h}-1\right)P + \Psi\right]. \tag{38}$$

Since $0<\xi bh<1$, in order to ensure $\dot{V}(t) \leq 0$, the positive error has to satisfy:

$$e \geq h\Psi + hP\left(\frac{1}{\xi\hat{b}h}-1\right) > 0. \tag{39}$$

when $e<0$,

$$\dot{V}(t) \leq -\frac{e^2}{h} + e\left[\left(\frac{1}{\xi\hat{b}h}-1\right)(-P) - \Psi\right].$$

In order to ensure $\dot{V}(t) \leq 0$, the negative error has to satisfy:

$$e \leq -h\Psi - hP\left(\frac{1}{\xi\hat{b}h}-1\right) < 0. \tag{40}$$

Eqs. (39) and (40) show that the wheel slip tracking error can be limited to a bounded range between $\pm[h\Psi + hP(1/\xi\hat{b}h-1)]$, but cannot converge asymptotically to zero. When the tuning parameter $\eta \to 0$, that is, much more weight is put on the slip tracking performance rather than minimization of the control effort, and when $\hat{b}=b$, $\xi\hat{b}h \to 1$, the boundary can just be reduced to $h\Psi$; when $\hat{b}^{-1}b \neq 1$, the boundary is also affected by the $\hat{b}^{-1}b$; especially, when $\hat{b}^{-1}b<1$, the boundary is enlarged severely. For a certain road surface, the target slip ratio is typically a constant (or at least piecewise constant), such that $\dot{\lambda}_d = 0$. Therefore, combining with (27), (31)

can be rewritten as

$$u(t) = -\frac{x_1}{h\hat{\varepsilon}_3}e - \frac{x_1}{\hat{\varepsilon}_3}\hat{f}(X). \tag{41}$$

The estimation error challenges the control system. For example, if the estimated value $|\hat{f}(X)|$ is selected much larger than the nominal value, the control input $u(t)$ will exceed its constraint; what is even worse is that the tracking error will be enlarged. This situation will be shown in Section 5.

To circumvent the perturbation term $x_1\hat{f}(X)/\hat{\varepsilon}_3$, and to make the tracking error converge asymptotically to zero, a feedback compensation term u_{fd} is designed based upon Assumption 3. Here, we redesign:

$$u(t) = -\frac{x_1}{h\hat{\varepsilon}_3}e + \frac{x_1}{\hat{\varepsilon}_3}u_{fd}. \tag{42}$$

Considering (32), (37), and substitute (42) into (24), we have

$$\dot{V}(t) = -\frac{e^2}{h}\zeta_0 + e\left[f(X) + u_{fd}\zeta_0\right]. \tag{43}$$

From (32), we know that $f(X)$ is bounded by $\zeta\alpha^T\beta(t)$, then, based on the Lyapunov function, we select:

$$u_{fd} = -\hat{\alpha}^T\beta(t)\mathrm{sgn}(e), \tag{44}$$

where, $\hat{\alpha}$ denotes the estimated vector set in the controller. It consists of the estimated vehicle parameters with each element $\hat{\alpha}_i > \alpha_i > 0$. And the control input can be written as

$$u(t) = -\frac{x_1}{h\hat{\varepsilon}_3}e - \hat{\theta}^T\delta(t)\mathrm{sgn}(e).$$

In order to reduce the chattering problem caused by the $\mathrm{sgn}(e)$, the control input $u(t)$ is redesigned as [36,37]

$$u(t) = \begin{cases} A(x_1)e - (\hat{\theta}^T\delta(t))^2\dfrac{e}{\gamma} & if\left|e\right| \le \gamma/\hat{\theta}^T\delta(t) \\ A(x_1)e - \hat{\theta}^T\delta(t)\dfrac{e}{\left|e\right|} & if\left|e\right| \ge \gamma/\hat{\theta}^T\delta(t) \end{cases} \tag{45}$$

where $A(x_1) = -x_1/(h\hat{\varepsilon}_3)$ and γ is an auxiliary signal, which satisfies [37,38]

$\gamma = \varpi e^{-\varsigma t}$ for $\varpi > 0,\ \varsigma > 0$;

$\hat{\theta}_i = \hat{\alpha}_i/\hat{\varepsilon}_3$;

$\delta^T(t) = \left[x_1^2\left|1-\lambda\right| \quad \left|\mu(x_3)(1-\lambda)\right| \quad \left|\mu(\lambda)\right| \quad \left|x_2\right|\right]$.

4. Brake torque distribution strategy

The brake torque distribution strategy is crucial to the braking performance and the RB efficiency. The structure of the entire control system is shown in Fig. 4. As illustrated, the supervisory slip controller first figures out the total torque requirement. Then, through the torque distributor, desired HB torque and RB torque can be obtained based on some criteria, for example, input/state constraints. Some mathematical methods can be used to solve the torque

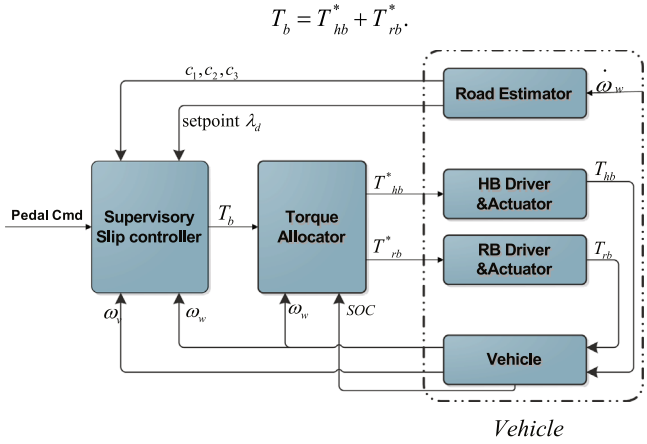

Fig. 4. Structure of the wheel slip control system.

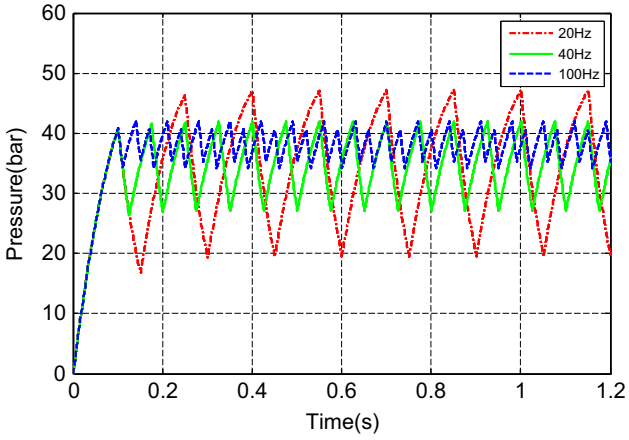

Fig. 5. Pressure response due to carrier frequency change (at 50% duty cycle).

allocation problem [39], for example, control allocation based on constrained quadratic programming (CQP) in [40], where

$$T_b = T^*_{hb} + T^*_{rb}. \tag{46}$$

Furthermore, in a conventional braking system, due to the on-off feature and the poor dynamic response, continuous modulation of the brake torque may lead to fluctuation in the master cylinder pressure, thus affecting the brake pedal feeling. As can be seen in Fig. 5, the frequency has a direct relationship with the pressure performance [18] and when the frequency is 20 Hz at a 50% duty-cycle, the difference of the maximum and minimum pressure can be 15 bar, which may undermine the torque control performance. Although the variable duty-cycle can reduce the fluctuation, the low carrier pulse in a conventional ABS still seriously affects the track performance, which will be detailed in Section 5. Some researchers have adopted pedal simulators to address this issue [41,42]. However, the pedal simulator may cause safety issue if the simulator sends incorrect information. In this paper,

we propose a novel approach that can not only deal with the pedal fluctuation problem without changing the conventional pedal structure, but also enhance the wheel slip tracking performance by blending RB into the braking system.

It is important to point out that the RB system can respond rapidly, yet it has a limited torque range and the torque is related to wheel angular speed [3,4]. In what follows, we design a strategy to combine the advantages of the large torque that HB system can output and the fast response that RB system can provide. The strategy is: the HB system generates a relatively stable pressure T^*_{hb}, and by adding the quickly-varying RB torque T^*_{rb}, the mixed torque can track the desired total brake toque T_b more closely. The task therefore becomes choosing a proper target HB torqueT^*_{hb}.

From Fig. 6, we know the highest friction coefficient exists when $\dot{\lambda}=0$ [44]. The slip ratio equilibrium point is the desired value for the control system. Hence, we are interested in the brake torque corresponded to the slip ratio equilibrium point. When neglecting the aerodynamic forces, the viscous friction force in (15) and substituting $\dot{\lambda}=0$, we have

$$\overline{T}_b=(mgr+\frac{Jg}{r_{eff}}(1-\overline{\lambda}))\mu(\overline{\lambda}). \tag{47}$$

where $\overline{\lambda}$ is the slip ratio equilibrium point characterized by $\dot{\lambda}=0$. $\overline{T}_b$ is the brake torque corresponding to the slip ratio equilibrium point. Then we choose,

$$T^*_{hb}=\overline{T}_b. \tag{48}$$

Note that due to the integration of quickly-varying RB torque, the small $\overline{T}_b$ calculation error caused by neglecting aerodynamic forces and the viscous friction force will not affect the brake performance. And actually, the aerodynamic forces and the viscous friction force have been taken into account in the controller design section.

Remark 2. In the control design part, the control law and torque distribution are designed and the related fault detection and isolation module will be developed in future with the framework proposed in [16].

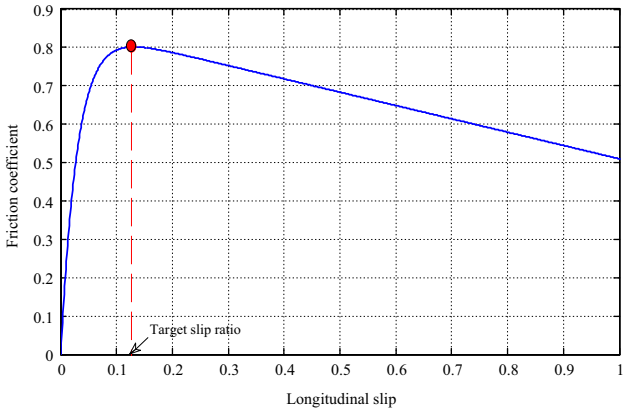

Fig. 6. $\mu-\lambda$ curve on wet asphalt surface.

5. Simulations and discussions

Simulation studies are conducted to evaluate the performance of the proposed controller and the torque distribution strategy. Firstly, we analyze the performance of the supervisory controller without considering the actuators dynamics. In this paper, the longitudinal speed ω_v is assumed to be available from an integrated dual-antenna differential global positioning system (DGPS) [26]. An active speed sensor and a tooth-wheel can be mounted on each of the four wheels to measure the wheel speed ω_w. The hydraulic cylinder pressure can be measured by pressure sensor M631T. Some of the parameters of the hybrid braking system in the quarter-car model are [4]: $m = 75$ kg, $J = 1.7$ kg m^2, $f_a = 0.03$ Ns$^2/m^2$, $f_v = 0$ Ns/rad.

5.1. Proposed supervisory controller

In this paper, a three-point prediction method is utilized to estimate the road surface. Based on (13), we know the slip ratio for the maximum friction coefficient can be given by $\lambda_{\mu\,\max} = \ln(c_1 c_2/c_3)/c_2$. And the road-surface parameters can be derived as [25]

$$c_1 = \frac{\mu(\lambda_1)\lambda_2 - \mu(\lambda_2)\lambda_1}{\lambda_2 - \lambda_1} \tag{49}$$

$$c_3 = \frac{\mu(\lambda_1) - \mu(\lambda_2)}{\lambda_2 - \lambda_1} \tag{50}$$

$$c_2 = \frac{\ln(c_1/(c_1 - \mu(\lambda_3) - c_3\lambda_3)}{\lambda_3} \tag{51}$$

where, $\lambda_1, \lambda_2, \lambda_3$ are three slip ratio constants to be chosen to estimate c_1, c_2, c_3; $\mu(\lambda_1)$,$\mu(\lambda_2)$, and $\mu(\lambda_3)$ are coefficients of friction at the respective slip ratios. In Fig. 7, the control performances of the proposed robust predictive control law with respect to various predictive time values are compared. As can be seen, the smaller tracking errors are related to the shorter predictive step. However, based on (45), we know if the predictive time value is too short, the control energy becomes oscillatory due to the $1/h$. In this paper, the predictive time is chosen to be 0.001.

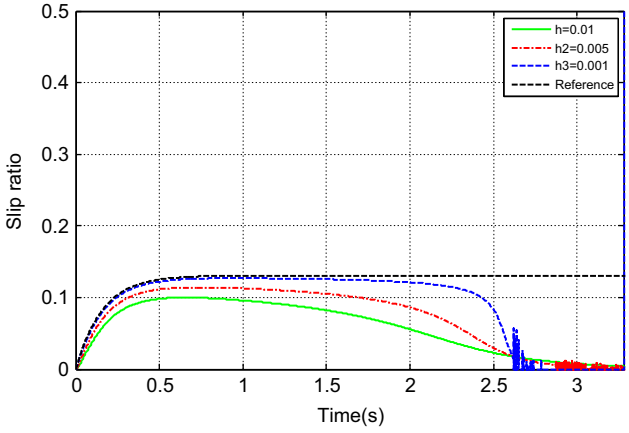

Fig. 7. Control performance with various predictive time value h.

In order to show the control performance of the proposed control law, the widely used sliding mode control (SMC) and a conventional proportional-integral (PI) controller are also utilized into the paper. For SMC method, the control law can be written as [43]

$$u = J\omega_v[-\hat{f}(\omega_v, \omega_w, \lambda) + \dot{\lambda}_d - k_H \mathrm{sgn}(e) - e/k_H], \tag{52}$$

$$k_H > (\eta + F)\hat{b}b^{-1} + \left|(\hat{b}b^{-1} - 1)u_{eq}\right| \tag{53}$$

where $|f - \hat{f}| \le F$, $u_{eq} = -\hat{f} + \dot{\lambda}_d, e(t) = \lambda(t) - \lambda_d(t)$ and k_H is the design parameter.

For the PI control method, the control input can be written as [4]

$$u = -k_p e(t) - k_i \int_0^t e(\tau)d\tau \tag{54}$$

where, k_p and $k_i$are the PI gains.

For the SMC method, k_H is chosen to be 1500. For the PI controller, $k_p = 3 \times 10^4$, $k_i = 5$. Fig. 8 shows the slip control performance between a SMC with chattering alleviation and the proposed controller while traveling on a wet asphalt surface. Based on the three-point estimation method mentioned above, the maximum friction coefficient can be attained. As can be observed from Fig. 8, both these two controllers can track the slip reference well; however, the proposed controller is able to track the reference signal with less error from Fig. 8. Also, we can find that the braking from the proposed controller is faster than the SMC method. Fig. 9 shows the performance comparison between a PI controller and the proposed one. Apparently, the braking time with the PI controller is nearly 0.5 s longer than the one with the proposed controller. Before 2.5 s, both PI and the proposed controllers show a good tracking performance. However, after 2.5 s, the slip ratio controlled by the PI method oscillates severely and the wheel is locked after 3s. This is probably because that, with the decrease of the vehicle speed, the slip ratio is too sensitive to be controlled well by the PI controller. From Figs. 8 and 9, we know the precision of all these three controllers will decrease with the reduction of the vehicle speed; however, the proposed one still outweighs the other two. Thus we can find that the proposed controller can improve the slip control performance during the emergency braking on the wet asphalt road. The corresponding angular wheel speed, vehicle speed, and the brake distance of the proposed controller are shown in Fig. 10. Note that in order to facilitate the comparison between the

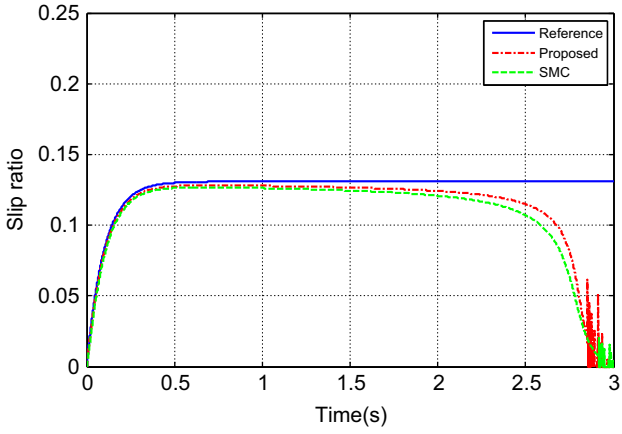

Fig. 8. Performance of the proposed controller and the SMC controller during an emergency brake (on wet asphalt).

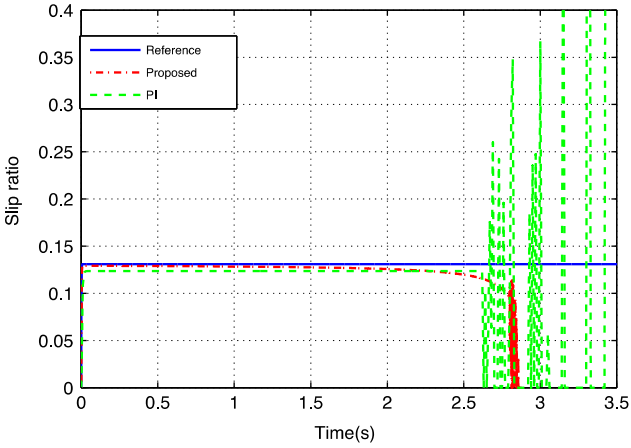

Fig. 9. Performance of the proposed controller and the PI controller during an emergency brake (on wet asphalt).

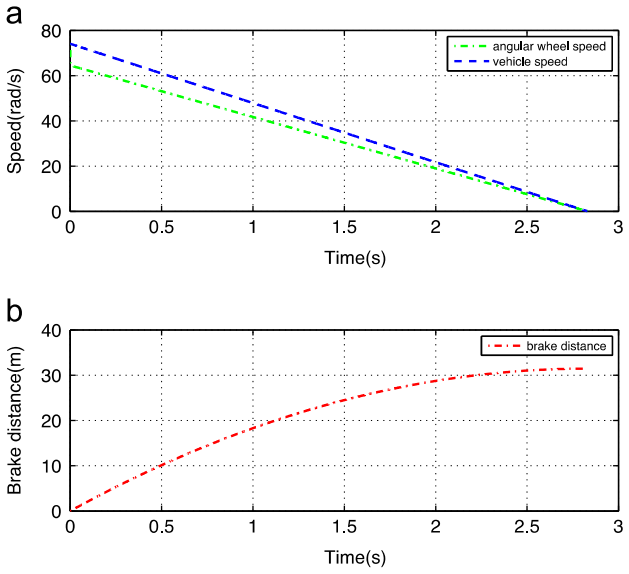

Fig. 10. The total performance of the proposed controller (on wet asphalt).

vehicle speed and wheel speed, the normal vehicle longitude speed unit (m/s) is transformed to the rad/s by dividing it with the wheel radius r_{eff}.

The performance comparisons among these three controllers on snow surface can be seen from Figs. 11 and 12. The desired slip ratio on snow surface is 0.06. As can be seen from Fig. 11, the proposed control method has less tracking error and shorter braking time compared with the SMC, though the braking time is much longer than that in dry road. Fig. 12 shows the slip ratio tracking performance between the PI and the proposed controller. We can see that the braking time with PI is nearly 3 s longer than the braking time with the proposed one. In addition, the slip ratio with the PI controller oscillates severely and the amplitude is rising with the decreasing of the vehicle momentum and the wheel is locked at 14 s, which may cause the vehicle to lose

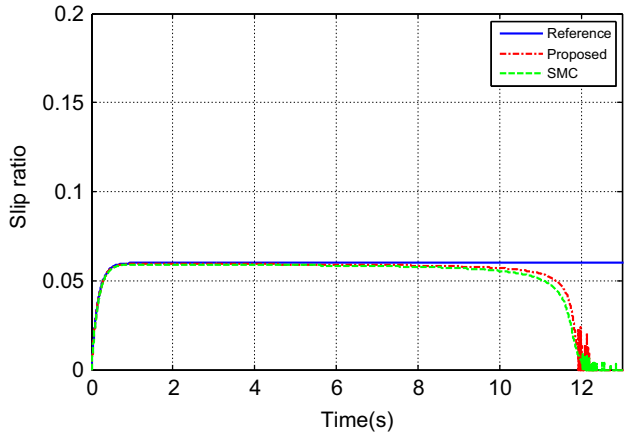

Fig. 11. Performance of the proposed controller and the SMC controller during an emergency brake (on snow).

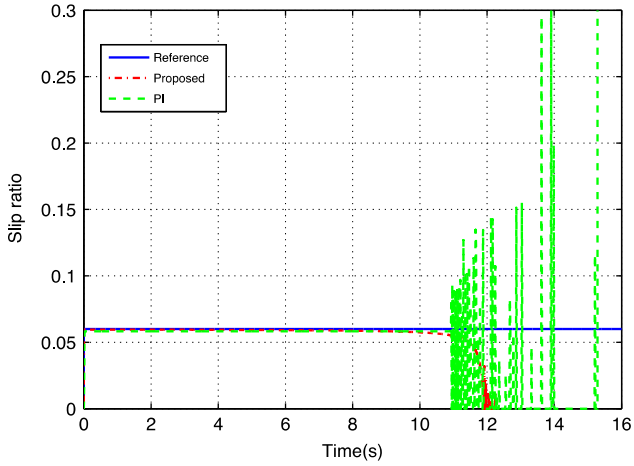

Fig. 12. Performance of the proposed controller and the PI controller during an emergency brake (on snow).

stability during braking. The total braking performance with the proposed controller is shown in Fig. 13. The normal vehicle longitude speed unit (m/s) in Fig. 13 is transformed to the unit (rad/s) based on the wheel radius r_{eff} to compare the difference between the wheel speed and vehicle speed. As can be seen, the vehicle speed is decreasing sharply and the wheel is not locked during the whole braking maneuver. The braking distance is 132.6 m which is 100.13 m longer than the braking distance on wet asphalt road as shown in Fig. 10.

In order to validate the proposed control law comprehensively, the brake performance results of these three controllers under various road surfaces are shown in Table 3. Braking distance is defined as the distance a vehicle travels from the point when brake is fully applied to when it comes to a complete stop. In this paper, braking distance S is derived by the integration of vehicle longitude speed (where $S = \int_0^t x_1 r_{eff} dt$). The item Ω denotes the square value of slip error (where, $\Omega = \kappa e^2$). In the braking performance evaluation, in addition to the braking distance, wheel slip ratio tracking error is also important because during an emergency braking

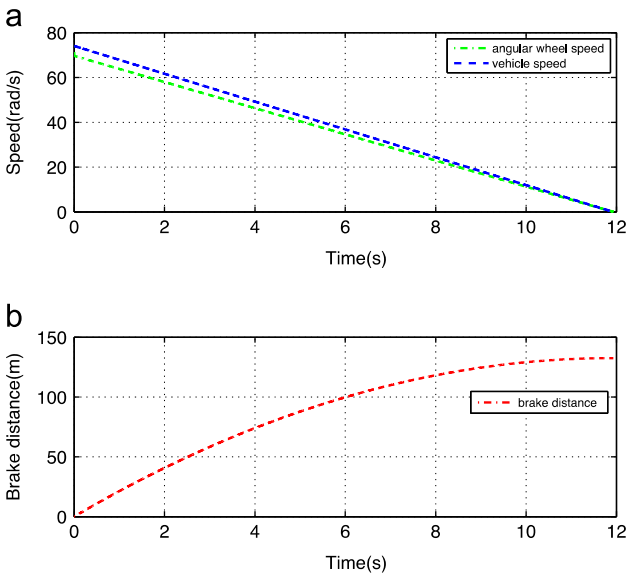

Fig. 13. The total performance of the proposed controller (on snow).

Table 3
Brake performance comparison for various surfaces.

Road	Control method	S (m)	Ω
Wet asphalt	Proposed	31.47	0.106
	SMC	31.57	0.471
	PI	31.69	1.873
Dry concrete	Proposed	23.14	0.150
	SMC	23.25	1.180
	PI	23.40	5.815
Cobble dry	Proposed	25.22	0.138
	SMC	25.26	2.220
	PI	25.38	6.764
Snow	Proposed	132.6	0.112
	SMC	132.7	0.373
	PI	134.0	11.47

maneuver, the slip tracking error directly affects the braking stability. Though the longitudinal tire force can still be high when the wheel is locked, the lateral tire force potential decreases sharply which could lead to dangerous situation [45], such as drifting. Table 3 shows the simulation results on various road surfaces with the initial speed 80 km/h and κ as 100. On the wet asphalt road, the braking distance from the proposed controller is 0.10 m better than the one from SMC, 0.2 m better than the one from PI; the slip ratio error index from the proposed one is nearly 25% of the SMC error and only 5% of the PI error, which denotes that the proposed controller improves the braking stability. Also can be seen in Fig. 9, the wheel is nearly locked after 3 s with the PI controller. On the dry road surface, compared with the wet asphalt road, due to the larger road friction coefficient, all of these three braking distances from these controllers

are reduced sharply. The braking performance results are similar with the ones on wet asphalt road surface, with the proposed controller giving the shortest braking distance and smallest slip ratio error. The error index in the proposed is just 10% of the SMC one and 2% of the PI one. On the cobble dry road, though the proposed one has the best performance, the braking distance differences and tracking error between the proposed and SMC are not very obvious. However, for the κe^2, the value by the proposed one is still very small, which is nearly 5% of the one by SMC and 2% of the one by PI controller. On the snow surface, it can be seen that all the braking distance values are longer than 100 m, which implies that the braking distance is affected mainly by the surface coefficient no matter how good the control performance is. However, it is still apparent that the proposed one outperforms the other two. Note that in the low coefficient road surface, the braking distance and error index under the PI controller are 1.4 m longer and 100 times larger than the proposed one, respectively.

The wheel slip ratio control performance between the OPC and the proposed control law with parameter estimation errors are compared in Figs. 14 and 15 for asphalt and snow road surfaces, respectively. In Fig. 14, one can see the performance comparisons between the OPC and the robust control laws in three parameters groups, namely A1, A2, and A3. For A1, the parameters satisfy $\hat{m} = 3$ m and $\hat{J} = 0.1$ J. As can be seen from Fig. 14(a), both the OPC and the proposed robust one show good tracking performance before 1 s. However, after that the slip ratio with OPC diverges from the reference and the wheel is locked at 2.8 s while the robust one still tracks the reference well. As mentioned before, with the increasing of the slip ratio, the lateral tire force decreases sharply which affects the vehicle stability. For A2, the parameters satisfy $\hat{m} = 1.5$ m and $\hat{J} = 3$ J. The Opc2 curve diverges from the reference from 0.1 s and oscillates severely during all the braking maneuver as shown in Fig. 14(b); for Robust2, the actual slip ratio tracking shows a good performance though there is an oscillation at the end of the braking due to the low

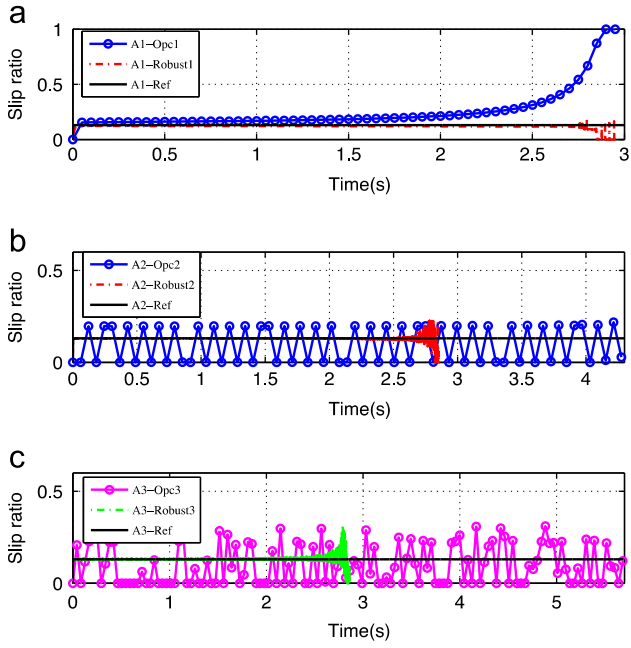

Fig. 14. The proposed control and the OPC method performance under estimation errors (on wet asphalt).

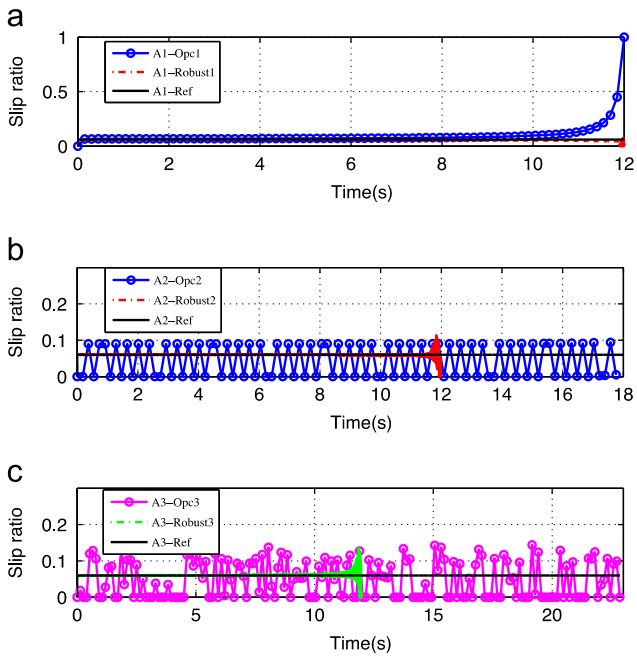

Fig. 15. The proposed control and the OPC method performance under estimation errors (on snow).

Table 4
Brake performance with parameters estimation errors on various surfaces.

Road	Control method	S (m)	Ω
Wet asphalt	Proposed	31.47	0.281
	OPC	47.97	4.592
Dry concrete	Proposed	23.14	0.448
	OPC	35.79	5.853
Cobble dry	Proposed	25.22	0.482
	OPC	41.66	40.25
Snow	Proposed	132.6	0.173
	OPC	200.6	4.472

vehicle speed. For A3, the parameters satisfy $\hat{m} = \text{m}$ and $\hat{J} = 4$ J. The performance comparisons are shown in Fig. 14(c) and it is apparent that both the slip error and the braking time in OPC are much larger and longer than those in the robust one. It takes the Opc3 nearly 6.0 s to stop the vehicle while for it just needs 2.8 s for Robust 3. The slip tracking error in Opc3 oscillates severely while the robust one shows a much better performance. On snow road surfaces, the robust control law still outperforms the OPC for all these three situations as shown in Fig. 15.

Table 4 shows the braking performance comparisons between OPC and the proposed one under various roads with estimation errors as $\hat{m} = 1.5$ m,$\hat{J} = 3$ J. When compared with the performance with no estimation errors shown in Table 3, the proposed one with estimation errors still presents a good braking performance. As can be seen in Table 4, in all these road surfaces, the proposed control law outperforms the OPC law. On wet asphalt surface, the proposed

controller can reduce 16.5 m braking distance compared with OPC and the corresponding tracking error index is nearly 6% of the OPC one. On dry concrete road, the braking distance from the proposed one is 12 m shorter than the OPC and the tracking error index with robust control is also rather smaller. On cobble road, the braking distance difference is 16 m and the slip error with OPC is nearly 98 times higher than the one in robust control. On snow road, due to the low friction coefficient, both these two controllers lead to longer braking distance values than those in other groups. As mentioned before, the slip error, especially on the low friction coefficient road surfaces, is much more important since the vehicle can be out of control easily when the wheels are locked. As can be seen, the proposed one shows a 0.173 tracking error while the OPC shows a higher value of 4.472 that is nearly 96 times higher than the robust one. When it comes to the braking distance, the proposed robust one shows a 132.6 m braking distance, 68 m shorter than the one with OPC. As can be seen from Fig. 15(c), due to the poor slip ratio tracking performance, the OPC takes nearly 24 s to stop the vehicle while for the proposed one can stop the car stably and quickly. From Table 4, it is apparent that the proposed robust one outperforms the OPC method when there are parameter estimation errors.

5.2. Torque allocation between RB and HB

According to the structure of the control strategy shown in Fig. 4, we will study the torque allocation here. However, firstly we will study the brake performance that the hydraulic braking system works isolatedly under the proposed supervisory controller. According to the structure of the control system in Fig. 4, the supervisory controller will compute the desired torque in real-time based on the road knowledge and the vehicle information, e.g. angular wheel speed.

Fig. 16 shows the simulation results that the conventional hydraulic braking system works independently without the RB system. Carrier pulse frequency in a conventional ABS system is usually around 20 Hz with variable duty-cycles. The hydraulic system can track the desired slip ratio as shown in Fig. 16 but not as good as the performance showed in Fig. 8 due to the actuator characteristics. In Fig. 17, we analyze the reasons for the performance difference from braking torque. As can be seen from Fig. 17(a), the control input T_b with HB system (input-w) is very

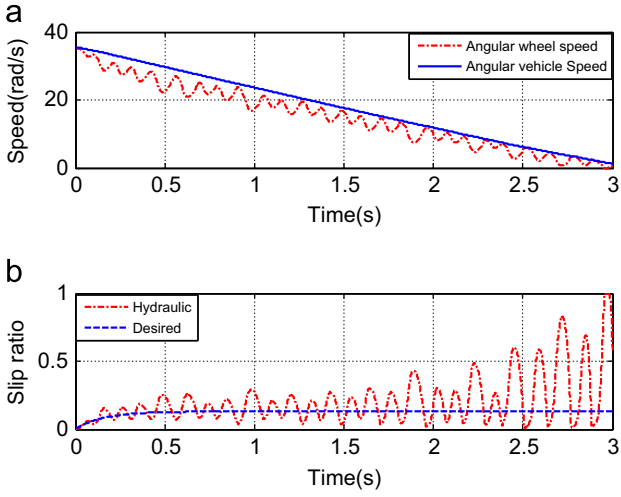

Fig. 16. The brake performance under hydraulic ABS only.

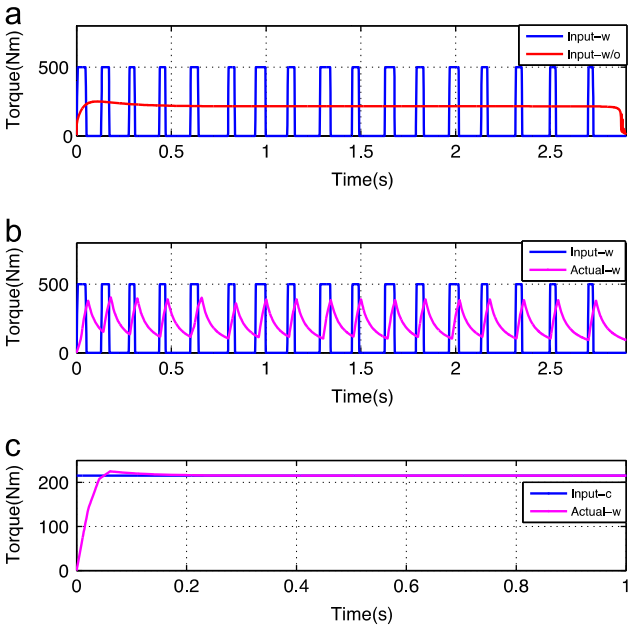

Fig. 17. The braking torque comparison between with and without HB system.

different from the control input without HB system (input-w/o). Based on (45) and Fig. 4, we know that the control input is affected directly by the vehicle speed x_1, actual slip ratio λ, and the tracking error. Compared with Figs. 9 and 10 (input-w/o), the vehicle speed x_1, actual slip ratio λ, and the tracking error in Fig. 16 account for the different control inputs between T_b with HB system (input-w) and T_b without HB system (input-w/o) showing in Fig. 17(a). In Fig. 17(b), we find that when only the HB system works, due to the slow HB actuator dynamic response, the actual HB torque (actual-w) will be significantly deformed. If the control input is a constant value (input-c) as shown in Fig. 17(c), the actual HB torque (actual-w) can tracks it well though there is a delay in the very beginning. Hence, a constant hydraulic braking torque reference T^*_{hb} is set in the system, which can be reached exactly without oscillations. And the torque difference between the T_b and T^*_{hb} can be compensated by the RB system [3,4].

In the following part, we will address this problem by the control strategy shown in Fig. 4. The main objective of control system is to track the slip reference and reduce brake distance, so the value of T^*_{hb} should make the actual slip ratio close to the reference as soon as possible. As analyzed in Section 4, T^*_{hb} is derived by (47) based on the slip ratio equilibrium point. From Fig. 18(a), we can find that the hydraulic brake torque keeps nearly a constant after 0.12 s. The mixed torque tracks the desired torque closely until 2.7 s. At this time, the vehicle has a very low speed where the slip ratio control could be deactivated and the wheel is allowed to be locked. Fig. 18(b) shows the zoom-in situation, where we can see at the very beginning the hydraulic torque is increasing very slowly due to the system characteristics while the mixed system has a faster response due to the RB (shown in Fig. 19) features. Noticeably from Fig. 18 the hydraulic braking torque is controlled as nearly a constant value, which implies that the hydraulic pressure has little fluctuation during this braking maneuver. Therefore, the pedal pulsating problem caused by the hydraulic pressure fluctuation can be eliminated under this control strategy, and at the same time the brake performance is guaranteed by the quick response provided by the RB as

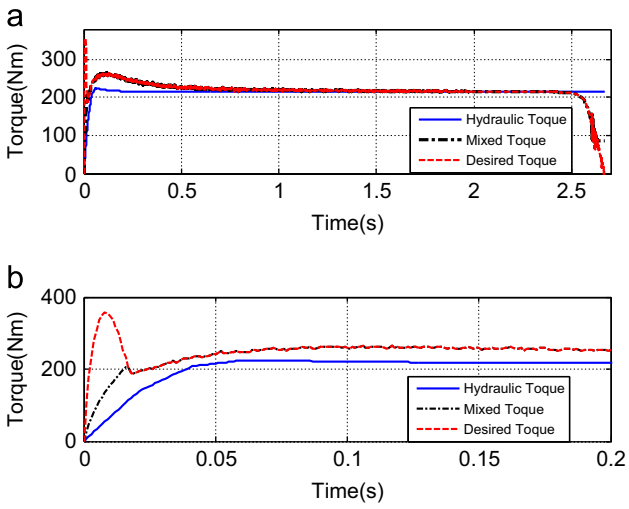

Fig. 18. Comparison of torque command with the actual total brake torque.

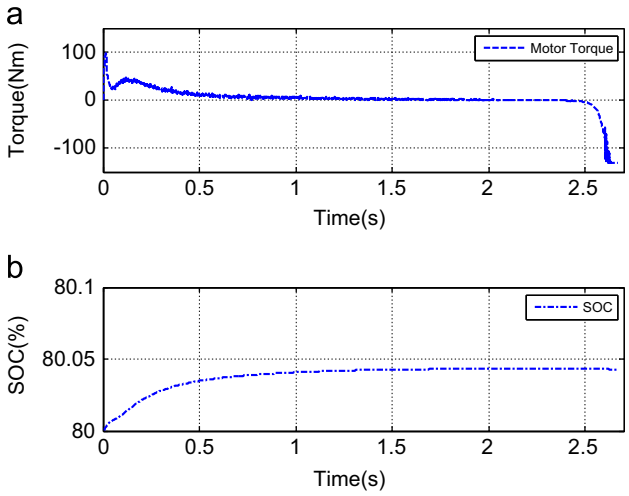

Fig. 19. Motor torque and the battery SOC.

shown in Fig. 18. In the period 0–0.01 s, there is a tracking error between the mixed torque and the desired one. That is because the control signal is faster than the response of this two actuator. However, this may not affect the performance since after 0.01 s the desired control input decreases and the mixed one tracks it well. The RB torque and battery SOC can be seen in Fig. 19. When the in-wheel motor system generates the brake torque or driving torque, the battery will be charged or discharged, respectively. From Fig. 20, we can see that the angular wheel speed has little fluctuation, and the difference between the angular wheel speed and vehicle speed decreases smoothly. Based on slip tracking performance shown in Fig. 20, we see under the proposed control method the desired slip ratio is successfully tracked by blending the HB and RB systems.

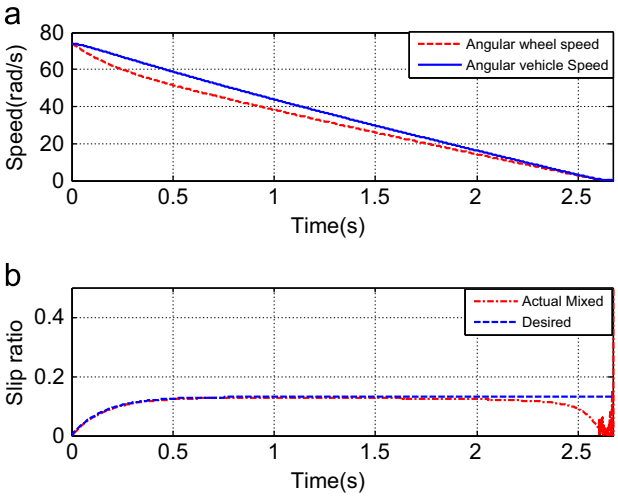

Fig. 20. Mixed torque control performance.

6. Conclusions

In this paper, a novel predictive-based robust controller has been proposed for tracking the desired wheel slip ratio to prevent wheel locking for IWMDEVs by combining the hydraulic and regenerative braking systems. The effectiveness of the proposed controller has been verified by carrying out extensive simulation studies. The proposed controller can track the reference slip ratio exactly and is robust for the vehicle parameter uncertainties. Based on the desired brake torque from the controller, a novel control strategy for allocating the torque between the HB and RB is proposed with the consideration of the actuator dynamics and the driving feeling. The simulation results show that the proposed system can not only track the wheel slip ratio well but also eliminate the hydraulic pressure pulsation which affects the driving feelings.

Acknowledgments

The work by Bin Wang, Xuexun Guo, and Xiaoyuan Zhu were partially supported by the Fundamental Research Funds for Central Universities (grant no. 2012-JL-11) and China Scholarship Council Funding.

References

[1] M. Schinkel, K. Hunt, Anti-lock braking control using a sliding mode like approach. In: Proceedings of American Control Conference, vol. 3, Anchorage, AK, May 8–10, 2002, pp. 2386–2391.

[2] M. Duoba, H. Ng, R. Larsen, Characterization and comparison of two hybrid electric vehicles (HEVs)-Honda Insight and Toyota Prius, SAE Technical. Paper, 2001-01-1335, 2001.

[3] R. Wang, Y. Chen, D. Feng, X. Huang, J. Wang., Development and performance characterization of an electric ground vehicle with independently actuated in-wheel motors, J. Power Sourc. 196 (8) (2011) 3962–3971pp 196 (2011) 3962–3971.

[4] X. Huang, J. Wang., Model predictive regenerative braking control for lightweight electric vehicles with in-wheel motors, Proc. Inst. Mech. Eng. Part D: J. Automob. Eng. 226 (9) (2012) 1220–1232.
[5] A. Walker, M. Lampérth, S. Wilkins, On friction braking demand with regenerative braking, SAE Technical. Paper 2002-01-2581, 2002.
[6] H. Yeo, S. Hwang, H. Kim, Regenerative braking algorithm for a hybrid electric vehicle with CVT ratio control, Proc. Inst. Mech. Eng. Part D: J. Automob. Eng. 220 (11) (2006) 1589–1600.
[7] J. Zhang, D. Kong, L. Chen, et al., Optimization of control strategy for regenerative braking of an electrified bus equipped with an anti-lock braking system, Proc. Inst. Mech. Eng. Part D: J. Automob. Eng. 226 (4) (2012) 494–506.
[8] C. Yu, T. Shim, Modeling of comprehensive electric drive system for a study of regenerative brake system. In: Proceedings of American Control Conference, Washington, DC, June 17–19, 2013, pp. 6749–6754.
[9] W.J.B. Midgley, H. Cathcart, D. Cebon., Modelling of hydraulic regenerative braking systems for heavy vehicles, Proc. Inst. Mech. Eng. Part D: J. Automob. Eng. 0 (0) (2013) 1–13.
[10] Rongrong Wang, Junmin Wang, Fault-tolerant control with active fault diagnosis for four-wheel independently-driven electric ground vehicles, IEEE Trans. Veh. Technol. 60 (9) (2011) 4276–4287.
[11] T.K. Bera, K. Bhattacharya, A.K. Samantaray, Bond graph model-based evaluation of a sliding mode controller for a combined regenerative and antilock braking system, Proc. Inst. Mech. Eng. Part I J. Syst. Control Eng. 225 (7) (2011) 918–934.
[12] D. Peng, Y. Zhang, G.-L. Yin, et al., Combined control of a regenerative braking and antilock braking system for hybrid electric vehicles, Int. J. Autom. Technol. 9 (6) (2008) 749–757.
[13] Shen Yin, H.a.o. Luo, S.X. Ding, Real-time implementation of fault-tolerant control systems with performance optimization, IEEE Trans. Ind. Electron. 61 (5) (2014) 2402–2411.
[14] Shen Yin, et al., A comparison study of basic data-driven fault diagnosis and process monitoring methods on the benchmark Tennessee Eastman process, J. Process Control 22 (9) (2012) 1567–1581.
[15] Shen Yin, et al., Data-driven monitoring for stochastic systems and its application on batch process, Int. J. Syst. Sci. 44.7 (2013) 1366–1376.
[16] Y.i.n. Shen, Guang Wang, Hamid Reza Karimi, Data-driven design of robust fault detection system for wind turbines, Mechatronics 24 (4) (2014) 298–306.
[17] Fengjun Yan, Junmin Wang, Kaisheng Huang, Hybrid electric vehicle model predictive control torque-split strategy incorporating engine transient characteristics, IEEE Trans. Veh. Technol. 61.6 (2012) 2458–2467.
[18] H.S. Jeong, H.E. Kim., Experimental based analysis of the pressure control characteristics of an oil hydraulic three-way on/off solenoid valve controlled by PWM signal, J. Dyn. Syst. Meas. Control 124 (1) (2012) 196–205pp 124 (2012) 196–205.
[19] J. Gerdes Christian, J. Karl Hadrick, Brake system modeling for simulation and control, Trans.-Am. Soc. Mech. Eng. J. Dyn. Syst. Meas. Control 121 (1999) 496–503pp 121 (1999) 496–503.
[20] C. Unsal, P. Kachroo, Sliding mode measurement feedback control for antilock braking systems, IEEE Trans. Control Syst. Technol. 7 (2) (1999) 271–281.
[21] S. Anwar, Anti-lock braking control of a hybrid brake-by-wire system, Proc. Inst. Mech. Eng. Part D J. Automob. Eng. 220 (8) (2006) 1101–1117.
[22] S.M. Savaresi, M. Tanelli, C. Cantoni, Mixed slip-deceleration control in automotive braking systems, J. Dyn. Syst. Meas. Control 129 (1) (2007) 20–31pp 129 (2007) 20–31.
[23] H. Mirzaeinejad, M. Mehdi, A novel method for non-linear control of wheel slip in anti-lock braking systems, Control Eng. Prac. 18 (8) (2010) 918–926.
[24] R. Wang, J. Wang, Tire-road friction coefficient and tire cornering stiffness estimation based on longitudinal tire force difference generation, Control Eng. Prac. 21 (1) (2013) 65–75.
[25] R. Bhandari, S. Patil, R.K. Singh, Surface prediction and control algorithms for anti-lock brake system, Transp. Res. Part C: Emerg. Technol. 21 (1) (2012) 181–195.
[26] Xiaoyu Huang, Junmin Wang, Center of gravity height real-time estimation for lightweight vehicles using tire instant effective radius, Control Eng. Prac. 21.4 (2013) 370–380.
[27] Lin-Hui Zhao, Zhi-Yuan Liu, Hong Chen, Design of a nonlinear observer for vehicle velocity estimation and experiments, IEEE Trans. Control Syst. Technol. 19.3 (2011) 664–672.
[28] T.A. Johansen, I. Petersen, J. Kalkkuhl, et al., Gain-scheduled wheel slip control in automotive brake systems, IEEE Trans. Control Syst. Technol. 11 (6) (2003) 799–811.
[29] Chen Chih-Keng, Development of fuzzy controlled ABS systems for motorcycles, Int. J. Veh. Des. 34.1 (2004) 84–100.
[30] M. Mitschke, H. Wallentowitz, Dynamik der Kraftfahrzeuge, 4th ed., Springer Verlag, Berlin, 2004.

[31] M. Mirzaei, G. Alizadeh, M. Eslamian, et al., An optimal approach to non-linear control of vehicle yaw dynamics, Proc. Inst. Mech. Eng. Part I: J. Syst. Control Eng. 222 (4) (2008) 217–229.
[32] W.H. Chen, D.J. Balance, P.J. Gawthrop, Optimal control of nonlinear systems: a predictive control approach, Automatica 39 (4) (2003) 633–641.
[33] H. Zhang, Y. Shi, S. Mehr, A robust H∞ PID control for multivariable networked control systems with disturbance/noise attenuation, Int. J. Robust Nonlinear Control 22 (2) (2012) 183–204.
[34] H. Zhang, J. Wang, Y. Shi, Robust H∞ sliding-mode control for Markovian jump systems subject to intermittent observations and partially known transition probabilities, Syst. Control Lett. 62 (12) (2013) 1114–1124.
[35] J.S. Yu, A robust adaptive wheel-slip controller for antilock brake system. In: Proceedings of the IEEE Conference on 36th Decision and Control, vol. 3, California, December1997, pp. 2545–2546.
[36] Pushkin Kachroo, Masayoshi Tomizuka, Chattering reduction and error convergence in the sliding-mode control of a class of nonlinear systems, IEEE Trans. Autom. Control 41.7 (1996) 1063–1068.
[37] L.C. Fu, Robust adaptive decentralized control of robot manipulators, IEEE Trans. Autom. Control 37 (1) (1992) 106–110.
[38] Bin Wang, Xiaoyu Huang, Junmin Wang, Xuexun Guo, Xiaoyuan Zhu, A robust wheel slip control design for in-wheel-motor-driven electric vehicles with hydraulic and regenerative braking systems. In: Proceedings of the 2014 American Control Conference, 2014, pp. 3225–3230.
[39] H.u.i. Zhang, Xinjie Zhang, Junmin Wang, Robust gain-scheduling energy-to-peak control of vehicle lateral dynamics stabilisation, Veh. System Dyn. 52 (3) (2014) 309–340.
[40] O. Härkegård, Dynamic control allocation using constrained quadratic programming, J. Guid. Control Dyn. 27 (6) (2004) 1028–1034pp 27 (2004) 1028–1034.
[41] K. Park, S.J. Heo, A study on the brake-by-wire system using hardware-in-the-loop simulation, Int. J. Veh. Des. 36 (1) (2004) 38–49pp 36 (2004) 38–49.
[42] D.F. Reuter, E.W. Lloyd, J.W. Zehnder, et al., A hydraulic design considerations for EHB systems, SAE Technical. Paper 2003-01-0324, 2003.
[43] Bin Wang, Xuexun Guo, Chengcai Zhang, Zhe Xiong, Huan Xia, and Jie Zhang, Slide Mode Control for Integrated Electric Parking Brake System, Math. Prob. Eng. vol. 2013 (Year 2013), Article ID 216982, 11 pages, http://dx.doi.org/10.1155/2013/216982.
[44] Sergio M. Savaresi, Mara Tanelli, Carlo Cantoni, Mixed slip-deceleration control in automotive braking systems, J. Dyn. Syst. Meas. Control 129 (1) (2007) 20–31.
[45] Erkin Dinçmen, B.A. Guvenc, Tankut Acarman, Extremum-seeking control of ABS braking in road vehicles with lateral force improvement, IEEE Trans. Control Syst. Technol. 22.1 (2014) 230–237.
[46] Rongrong Wang, Junmin Wang, Fault-tolerant control for electric ground vehicles with independently-actuated in-wheel motors, ASME Trans. J. Dyn. Syst. Meas. Control 134 (2) (2012) 021014 (10 pages).